INTERNAL HEAT SOURCES
IN LARGE STRAIN THERMO-ELASTO-PLASTICITY
– THEORY AND FINITE ELEMENT SIMULATIONS[1]

BALBINA WCISŁO

Cracow University of Technology, Chair of Computational Engineering, Cracow, Poland

e-mail: balbina.wcislo@pk.edu.pl

MARZENA MUCHA

Cracow University of Technology, Chair of Computational Engineering, Cracow, Poland, and

TU Dortmund University, Institute of Mechanics, Department of Mechanical Engineering, Dortmund, Germany

JERZY PAMIN

Cracow University of Technology, Chair of Computational Engineering, Cracow, Poland

The paper deals with theoretical description and numerical simulations of internal sources of heating/cooling in large strain thermo-elasticity and thermo-elasto-plasticity. The attention is paid to metallic materials which undergo cooling in the elastic range and heating during plastic yielding. Theoretical description can be derived from thermodynamic considerations based on the first and second laws of thermodynamics and assumed forms of the Helmholtz free energy. Numerical simulations within the Finite Element Method are performed for a uniaxial tension test and elongation of a dogbone-shape sample. For the latter specimen, a comparison with experimental results is performed, and good agreement is obtained.

Keywords: thermo-mechanics, thermo-elastic cooling, plastic dissipation, AceGen/FEM

1. Introduction

In non-isothermal conditions, the response of an elastic-plastic material is usually described by using two governing equations: the balance of linear momentum and the balance of energy. The equations can be coupled, the thermal field can influence the mechanical one, and conversely. In particular, a change of temperature causes thermal expansion of the material and influences material parameters, both the mechanical (e.g. Young's modulus or initial yield threshold) and thermal ones (e.g. heat conductivity or heat capacity coefficients). It should be noted that the decreasing value of the yield limit can lead to softening of the material and to strain localization, see e.g. Duszek and Perzyna (1991), which additionally complicates the constitutive description, since the response can then be incorrectly represented by a classical (local) constitutive theory.

On the other hand, large deformation of a sample can influence heat transfer in the material and can involve internal sources of heating or cooling. In particular, in the elastic regime, a thermo-elastic coupling, related to the Gough-Joule effect, can be observed. Very often, the phenomenon is related to so-called entropic materials like rubber or polymers, see Holzapfel (2000), which undergo heating during rapid stretching. However, it is observed in experiments that metals also show thermo-elastic coupling in the elastic regime but in a different way – their temperature decreases during elongation (Mucha *et al.*, 2023). A second example of the internal heat source in a material is plastic deformation which causes heat generation due to energy

---

[1]Paper presented during PCM-CMM 2023, Gliwice, Poland

dissipation. This matter is widely analysed in literature in the context of experiments, theory and simulations, for example (Taylor and Quinney, 1934; Ristinmaa *et al.*, 2007; Oliferuk *et al.*, 2013; Rose and Menzel, 2021; Musiał *et al.*, 2022).

The subject of this paper is the analysis of fully thermo-mechanically coupled elasto--plasticity, with special attention paid to internal heat sources observed in elastic and plastic regimes for materials undergoing large strains. The formulation is derived in a thermodynamically consistent manner on the basis of the Helmholtz free energy which consists of the following parts: reversible (including elasticity and thermal expansion), purely thermal and plastic. The internal heat sources related to the thermo-elastic coupling and to energy dissipation during yielding of the material can be derived from the first and second laws of thermodynamics according to, for example, Ristinmaa *et al.* (2007), Oppermann *et al.* (2022). A simplified specification of the plastic dissipation heat source, i.e. the application of the Taylor-Quinney factor, is also used for comparison.

The attention in the paper is focused on metals/alloys, and isotropy of the material is assumed. The thermo-mechanical coupling involves thermal expansion, internal heat sources in elasticity and plasticity, Fourier's law in the deformed configuration and thermal softening in plasticity. It does not include the dependence of material parameters on temperature. The description of plasticity in this work is based on Huber-Mises-Hencky theory with associative flow rule without viscous terms.

The presented model is implemented within the Finite Element Method (FEM) (Zienkiewicz *et al.*, 2005), and two specimens are tested: a cube and a dogbone-shape sample, both in tension. Simulations for the latter specimen are compared with the results of laboratory experiments presented in Mucha *et al.* (2023). Although in the experiments by (Mucha *et al.*, 2023) propagative instabilities are observed (i.e. the Lueders bands and Portevin-Le Chatelier effect), which are not reproduced by the presented model, the comparison of reactions and temperature is performed in a general way, and a good agreement is obtained.

The thermo-elastic and thermo-elasto-plastic models are described using different stress and strain measures. This approach is applied here intentionally: thermo-elasticity can easily be described using quantities related to the reference configuration, and this allows for efficient implementation within FEM. In turn, thermo-elasto-plasticity at large strain is based on plasticity description developed in (Simo and Hughes, 1998) and (Simo and Miehe, 1992), which involves spatial quantities, and can be effectively applied in the chosen FEM software (Korelc and Wriggers, 2016).

The large strain elasto-plasticity theory, which takes into account the full thermo-mechanical coupling, leads to strongly non-linear problems. Numerical simulations using such a material model require an advanced solution approach. In this work, finite element procedures are implemented within symbolic-numerical package AceGen for Wolfram Mathematica (Korelc and Wriggers, 2016). The most significant feature of the package is automatic differentiation which allows for computation of the tangent operator in the Newton-Raphson procedure as a derivative of the residual vector with respect to the vector of unknowns.

The paper is laid out as follows. In Section 2, basic quantities and thermodynamic laws are presented, which are further used in the specific models. In Section 3, the thermo-elastic model is presented with special attention paid to thermo-elastic coupling and its numerical simulation. The thermo-elasto-plastic model is presented, in turn, in Section 4. Two variants of the model are investigated using FEM, the first in which plastic dissipation is calculated directly from thermodynamic considerations and the second one related to the simplified approach with the Taylor-Quinney coefficient. The paper is closed with Section 5 including final remarks.

2. Fundamentals

The description of large strain kinematics applied in the presented model can be found e.g. in (Bonet and Wood, 2008; Haupt, 2002; Wriggers, 2008). Let us consider a deformable continuous body whose particles in the reference configuration occupy material points denoted with the vector $\mathbf{X}$. At a time t, the placement of the particle $\mathbf{X}$ in the current configuration is described with the vector $\mathbf{x}(\mathbf{X}, t)$. The displacement vector is defined as $\mathbf{u}(\mathbf{X}, t) = \mathbf{x}(\mathbf{X}, t) - \mathbf{X}$, whereas the deformation gradient and its determinant are

$$\mathbf{F} = \frac{\partial \mathbf{x}}{\partial \mathbf{X}} = \mathbf{I} + \frac{\partial \mathbf{u}}{\partial \mathbf{X}} \qquad J = \det(\mathbf{F}) \tag{2.1}$$

Symbol $\mathbf{I}$ in the above equation denotes the second-order identity tensor. The left Cauchy-Green deformation tensor, its determinant and the right Cauchy-Green deformation tensor are defined as follows

$$\mathbf{b} = \mathbf{F}\mathbf{F}^{\mathrm{T}} \qquad J^b = \det(\mathbf{b}) \qquad \mathbf{C} = \mathbf{F}^{\mathrm{T}}\mathbf{F} \tag{2.2}$$

The velocity of a particle is defined as the time derivative of $\mathbf{x}$ with respect to time $\mathbf{v} = \partial \mathbf{x}/\partial t = \partial \mathbf{u}/\partial t$.

The first law of thermodynamics in the referential setting has the form, see e.g. (Holzapfel, 2000; Simo, 1998)

$$\dot{e} = \mathbf{P} : \dot{\mathbf{F}} + \mathcal{R} - \mathrm{Div}\,(\mathbf{Q}) \tag{2.3}$$

where e is the internal energy per unit initial volume, the dot over symbol denotes time derivative (i.e. rate), $\mathbf{P}$ denotes the first Piola-Kirchhoff stress tensor, $\mathcal{R}$ is an external source of heat per unit of the initial volume, and $\mathbf{Q}$ is the Piola-Kirchhoff heat flux density vector (for detailed discussion on heat flux density measures, see Wcisło *et al.* (2023)). Symbol $\mathrm{Div}\,(\cdot)$ denotes the divergence of vector $\cdot$ in the reference configuration, and the colon is used for the scalar product of two second-order tensors.

The second law of thermodynamics in the form of Clausius-Duhem inequality reads (Truesdell and Toupin, 1960)

$$\dot{s} - \frac{\mathcal{R}}{T} + \mathrm{Div}\left(\frac{\mathbf{Q}}{T}\right) \geqslant 0 \tag{2.4}$$

where the rate of entropy (per unit of initial volume) is denoted with $\dot{s}$, and the absolute temperature with T.

The constitutive equation for the heat flow applied in this work is spatial Fourier's law for Kirchhoff heat flux density vector $\widehat{\mathbf{q}}$ which can be equivalently expressed using the Piola Kirchhoff heat flux, see (Wcisło *et al.*, 2023)

$$\widehat{\mathbf{q}} = -k\,\mathrm{grad}\,(T) \qquad \Longleftrightarrow \qquad \mathbf{Q} = -k\mathbf{C}^{-1}\,\mathrm{Grad}\,(T) \tag{2.5}$$

In the above equation, the parameter k is the heat conductivity of the material, whereas symbols $\mathrm{grad}\,(\cdot)$ and $\mathrm{Grad}\,(\cdot)$ denote the spatial and referential gradient of quantity $\cdot$, respectively.

The balance of linear momentum for the static case with mass forces neglected has the following form (Simo, 1998)

$$\mathrm{Div}\,(\mathbf{P}) = \mathbf{0} \tag{2.6}$$

3. Thermo-elasticity

3.1. Model of the thermo-elastic material

For the thermo-elastic material model, the free energy is assumed to be a function of the deformation gradient and temperature $\psi = \psi(\mathbf{F}, T)$. Using the Legendre transformation $\psi = e - Ts$, see e.g. (Marsden and Hughes, 1983), the following form of the second law of thermodynamics can be written

$$\Big[\mathbf{P} - \frac{\partial \psi}{\partial \mathbf{F}}\Big] : \dot{\mathbf{F}} - \Big[s + \frac{\partial \psi}{\partial T}\Big]\dot{T} - \frac{1}{T}\mathbf{Q} \cdot \operatorname{Grad}(T) \geqslant 0 \tag{3.1}$$

The state equations for the first Piola-Kirchhoff stress tensor and entropy are as follows

$$\mathbf{P} = \frac{\partial \psi}{\partial \mathbf{F}} \qquad s = -\frac{\partial \psi}{\partial T} \tag{3.2}$$

Then the reduced form of the second law of thermodynamics is obtained

$$\mathcal{D}_{therm} = -\frac{1}{T}\mathbf{Q} \cdot \operatorname{Grad}(T) \geqslant 0 \tag{3.3}$$

and it is fulfilled for the assumed Fourier law in Eq. (2.5).

Further derivations lead to temperature form of the energy balance equation

$$c\dot{T} + \operatorname{Div}(\mathbf{Q}) - \mathcal{R} - \mathcal{H} = 0 \qquad c = -T\frac{\partial^2 \psi}{\partial T^2} \qquad \mathcal{H} = T\frac{\partial^2 \psi}{\partial \mathbf{F}\partial T} : \dot{\mathbf{F}} \tag{3.4}$$

where c is the heat capacity per unit volume and $\mathcal{H}$ is a thermo-elastic source of heating/cooling.

In the following analysis, the specific form of the free energy function is applied, cf. (Simo and Miehe, 1992)

$$\psi(\mathbf{F}, T) = \widehat{\psi}(\mathbf{b}(\mathbf{F}), T) = \psi^{eT}(\mathbf{b}, T) + \psi^{T}(T) \tag{3.5}$$

The first component of the free energy ψ^{eT} is related to elastic deformation and thermal expansion, whereas the second component ψ^{eT} is the purely thermal part

$$\psi^{eT}(\mathbf{b}, T) = \frac{1}{2}K\ln^2(\sqrt{J^b}) + \frac{1}{2}G\Big[\operatorname{tr}([J^b]^{-1/3}\mathbf{b}) - 3\Big] - 3K\alpha_T(T - T_0)\ln(\sqrt{J^b})$$
$$\psi^{T}(T) = c_0\Big[(T - T_0) - T\ln Bigl(\frac{T}{T_0}\Big)\Big] \tag{3.6}$$

where K and G are the bulk and shear moduli, respectively, α_T is the coefficient of linear thermal expansion, c_0 is the initial specific heat capacity expressed per unit of material volume and T_0 is the initial (reference) temperature of the material. For the assumed form of the purely thermal part of the free energy function, the heat capacity in Eq. (3.4) equals $c = c_0$.

The thermo-elastic heating/cooling from Eq. (3.4) can now be derived as

$$\mathcal{H} = -3TK\alpha_T\mathbf{F}^{-1} : \dot{\mathbf{F}} \tag{3.7}$$

The value of $\mathcal{H}$ can be positive or negative: if $\mathbf{F}^{-1} : \dot{\mathbf{F}} < 0$ then the material undergoes heating, if $\mathbf{F}^{-1} : \dot{\mathbf{F}} > 0$ the material undergoes cooling. Note that the thermo-elastic heating/cooling is rate-dependent: the higher the rate of the deformation tensor, the greater effect of heating/cooling produced during deformation process. It is worth emphasizing that the thermo-elastic source of heating/cooling is dependent on the material parameters related to elasticity, i.e. the bulk modulus and thermal expansion, and there are no additional parameters which can control the heating/cooling source during elastic deformation.

3.2. Numerical simulations for thermo-elasticity

The thermo-elastic model presented in Section 3.1 is implemented within the FEM for a 3D space in *Wolfram Mathematica* packages AceGen/FEM (Korelc and Wriggers, 2016). The former package is a code generator capable of automatic differentiation, whereas the latter is a FEM engine.

The fundamental unknowns for the problem are displacement vector **u** and temperature T. For the two-field problem, hexahedral finite elements with linear interpolation of both unknown fields are applied. To avoid volumetric locking, the code includes the modification called *F-bar* (de Souza Neto *et al.*, 2008). The implementation aspects of thermomechanical models are discussed in (Wcisło and Pamin, 2017).

3.2.1. Uniaxial tension test

The first computations are performed for a uniaxial tension test simulated with one cubic finite element with dimensions $L = W = H = 10$ mm, see Fig. 1a. The mechanical boundary conditions are applied in such a way that the homogeneous stress state is preserved. The insulation on all sides of the cube is assumed. The enforced displacement has the maximum value ΔL=0.05 mm (the sample remains in the elastic regime) and is applied monotonically within 10 , 1 s or 0.1 s, thus there are three rates of elongation under consideration called further as slow, medium rate and fast processes. The following material data related to aluminium are used: $K = 57.133 \cdot 10^9$ Pa, $G = 26.369 \cdot 10^9$ Pa, $k = 121$ W/(m·K), $c_0 = 2.423 \cdot 10^6$ J/(m^3·K), $\alpha_T = 23.2 \cdot 10^{-4}$ K^{-1}.
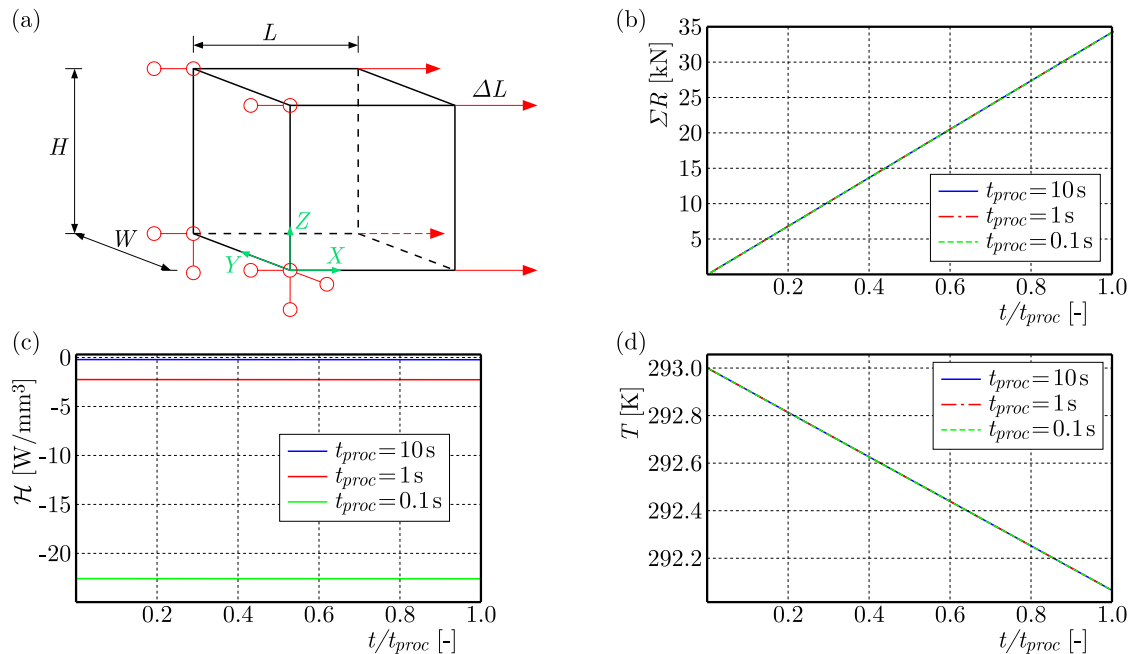

Fig. 1. Uniaxial tension test for 1 FE: (a) specimen and mechanical boundary conditions, (b) sum of reactions vs. time, (c) thermo-elastic source of heating/cooling vs. time, (d) temperature vs. time

The sum of reactions vs. (relative) process time is presented in Fig. 1b. The diagrams are almost linear, and for different elongation rates the curves coincide in spite of different values of thermo-elastic source of heating/cooling in Fig. 1c which depend on the process rate. It can be observed that the value of $\mathcal{H}$ is negative, thus indeed the tests reproduce the thermo-elastic cooling observed in metallic materials. The diagram presenting the evolution of temperature in the sample is shown in Fig. 1d. Although for different process rates, different intensity of cooling

is produced, and it does not influence the value of temperature in the sample. This behaviour can be explained by the fact that for the homogeneous temperature distribution in the sample, the energy balance in Eq. (3.4) reduces to equation $c\dot{T} = -3TK\alpha_T\mathbf{F}^{-1} : \dot{\mathbf{F}}$. The application of the backward Euler time integration $\dot{T} = (T - T_n)/\Delta t$ and $\dot{\mathbf{F}} = (\mathbf{F} - \mathbf{F}_n)/\Delta t$, where T and $\mathbf{F}$ are the values at the current time step, T_n and $\mathbf{F}_n$ are values from the previous time step, and Δt is the time increment, leads to the following closed-form formula for temperature at the current time step

$$T = T_n\Big[1 + \frac{3K\alpha_T\mathbf{F}^{-1} : (\mathbf{F} - \mathbf{F}_n)}{c}\Big]^{-1} \tag{3.8}$$

It can be noted that the current value of temperature does not depend directly on time, but only on the increment of deformation.

At this stage, it is worth mentioning that for the isotropic model, the thermo-elastic heating/cooling can also be alternatively calculated using formula (Simo and Miehe, 1992)

$$\mathcal{H} = T\frac{\partial^2\psi}{\partial J\partial T} : \dot{J} = -3TK\alpha_T\frac{1}{J}\dot{J} \tag{3.9}$$

In this case, the rate of determinant of the deformation gradient $\dot{J}$ can be approximated straightforwardly using formula $\dot{J} = (J - J_n)/\Delta t$. However, it can be shown, see e.g. (Bonet and Wood, 2008; Wood, 2008), that $\dot{J} = J\,\mathrm{tr}\,(\mathbf{d})$, where $\mathbf{d}$ is the symmetric part of the velocity gradient. If the velocity is approximated as $\mathbf{v} = (\mathbf{u} - \mathbf{u}_n)/\Delta t$ then the obtained results can be different. It has been tested numerically that for aluminium and the elastic range, the choice of approximation of $\dot{J}$ does not influence the results significantly.

3.2.2. *Dogbone sample – comparison with experiment in elastic range*

This Subsection includes a comparison of experiments and simulations performed for a dogbone-shape sample in tension. The description of the laboratory experiments, which are used here, can be found in (Mucha *et al.*, 2023). The sample of thickness 2 mm presented in Fig. 2 is made of aluminium AW5083. The applied material parameters are the same as for the uniaxial tension test in the previous Subsection. In the numerical tests, the specimen is insulated on all sides. The experiments reported in (Mucha *et al.*, 2023) were performed for three displacement rates: slow $6 \cdot 10^{-5}$ m/s (experiments No. 1, 2 and 3), medium rate $6 \cdot 10^{-4}$ m/s (experiments No. 4, 5 and 6) and fast $6 \cdot 10^{-3}$ m/s (experiments No. 7, 8 and 9). The comparison of experimental and numerical results is presented in Fig. 3. For clarity, the experimental results obtained for the same process rates are marked with the same colour but different line style.
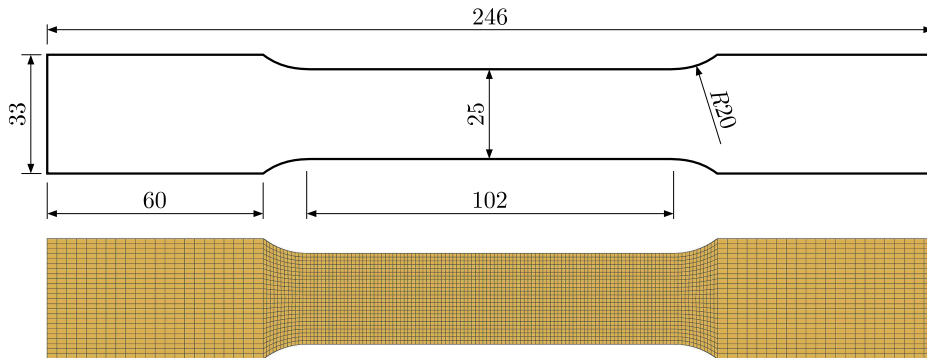

Fig. 2. Geometry, dimensions (in milimeters) and discretization of the dogbone sample
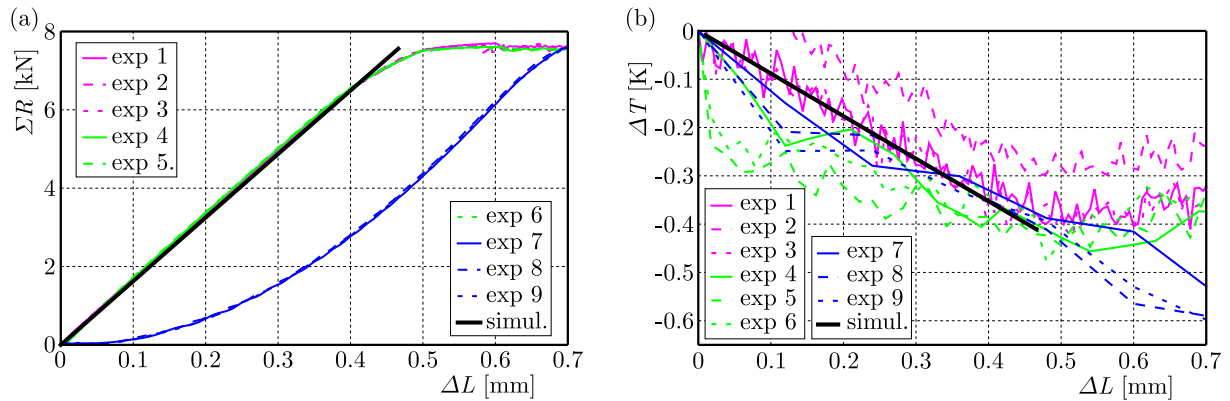
Fig. 3. Comparison of experiments and simulations for the dogbone sample in the elastic regime: (a) sum of reactions vs. enforced displacement, (b) temperature at the central material point of the sample vs. displacement

The constitutive model used for the simulation does not include viscous effects in the elastic regime, and only dependence of the material response on the process rate is related to thermo-elastic heating/cooling. However, in the analysed case, this factor has negligible influence on reactions, thus the black diagram in Fig. 3a is the result obtained for the three analysed rates. It can be observed that the reaction diagrams for simulations almost coincide with the experiments performed with slow and medium rates. In turn, the blue curves for the fast process are significantly different from the rest of results, which can be attributed to an unwanted loading machine effect.

The results of experiments presented in (Mucha *et al.*, 2023) include measurement of temperature on the surface at the central point of the sample. The comparison of experimental and simulation outcome is performed in Fig. 3b. Also in this case the results obtained from simulations performed for different displacement rates coincide (the black diagram). The reason is as follows: the simulated sample and boundary conditions are symmetric, thus the obtained temperature distribution is symmetric as well. As a result, at the central point of the sample the temperature gradient is zero, and taking the considerations from the previous Subsection into account, temperature is not dependent on the process rate. It can be observed in Fig. 3b that the numerical simulations reproduce temperature evolution at the center of the sample very well. The black line is in the middle of all experimental curves.
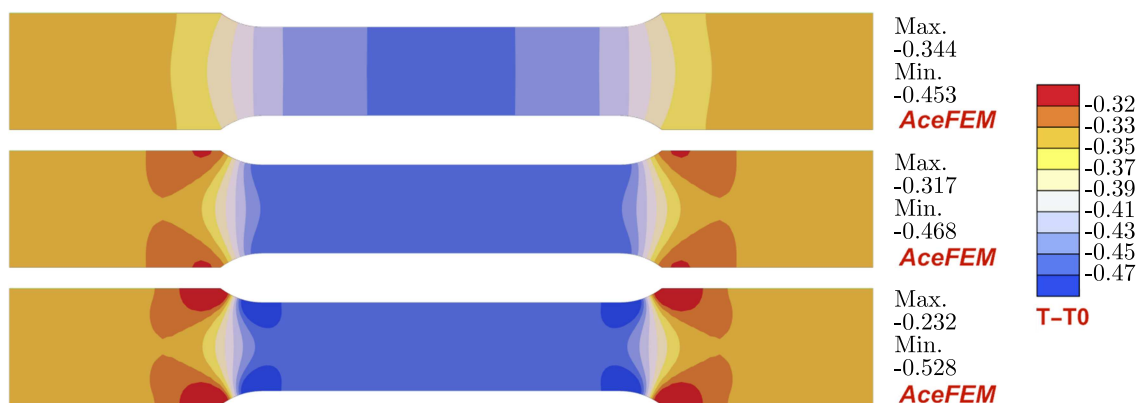

Fig. 4. Temperature distribution for slow, medium rate and fast processes (top, middle and bottom, respectively) at the end of simulation

Although at the central point of the sample temperature does not depend on the deformation rate, it is worthwhile to investigate its value obtained in simulations for the whole specimen.

Fig. 4 shows the temperature distribution at the end of simulation for the three analysed displacement rates. It can be observed that the whole sample undergoes cooling. In the central part of the specimen temperature is similar for each process rate, however significant differences are observed in the areas where the web widens. For the fast process, the difference between the minimum and maximum temperature is the highest.

4. Thermo-elasto-plasticity

4.1. Model of thermo-elasto-plastic material

The description of the thermo-elasto-plastic material is based on the assumption of multiplicative decomposition of the deformation gradient into a reversible part (related to elastic deformation and thermal expansion) and a plastic part $\mathbf{F} = \mathbf{F}^r\mathbf{F}^p$, see (Ristinmaa *et al.*, 2007), although an alternative formula $\mathbf{F} = \mathbf{F}^\theta\mathbf{F}^e\mathbf{F}^p$, where $\mathbf{F}^\theta$ is a thermal part and $\mathbf{F}^e$ an elastic one could also be applied, cf. (Wcisło and Pamin, 2017). Now, the left reversible Cauchy-Green deformation tensor and its determinant are defined as

$$\mathbf{b}^r = \mathbf{F}^r[\mathbf{F}^r]^{\mathrm{T}} \qquad J^{br} = \det(\mathbf{b}^r) \tag{4.1}$$

Further, the spatial velocity gradient and its decomposition are written, cf. (Ristinmaa *et al.*, 2007)

$$\mathbf{l} = \dot{\mathbf{F}}\mathbf{F}^{-1} \qquad \mathbf{l} = \mathbf{l}^r + \mathbf{l}^p \qquad \mathbf{l}^r = \dot{\mathbf{F}}^r[\mathbf{F}^r]^{-1} \qquad \mathbf{l}^p = \mathbf{F}^r\dot{\mathbf{F}}^p[\mathbf{F}^p]^{-1}[\mathbf{F}^r]^{-1} \tag{4.2}$$

The symmetric part of the velocity gradient and its plastic part are as follows

$$\mathbf{d} = \operatorname{sym}(\mathbf{l}) \qquad \mathbf{d}^p = \operatorname{sym}(\mathbf{l}^p) \tag{4.3}$$

The Helmholtz free energy for the isotropic thermo-elasto-plastic material is assumed here as a function of the left reversible Cauchy-Green deformation tensor, internal variable associated with isotropic hardening α and temperature: $\psi = \psi(\mathbf{b}^r, \alpha, T)$, see (Ristinmaa *et al.*, 2007). The dissipation inequality for this case is

$$\mathcal{D} = \boldsymbol{\tau} : \mathbf{d} - s\dot{T} - \dot{\psi} - \frac{1}{T}\mathbf{Q} \cdot \operatorname{Grad}(T) \geqslant 0 \tag{4.4}$$

where $\boldsymbol{\tau}$ is the Kirchhoff stress tensor. After derivations, the above equation can be presented in the following form

$$\mathcal{D} = \left[\boldsymbol{\tau} - 2\frac{\partial\psi}{\partial\mathbf{b}^r}\mathbf{b}^r\right] : \mathbf{d} + 2\frac{\partial\psi}{\partial\mathbf{b}^r}\mathbf{b}^r : \mathbf{d}^p - \frac{\partial\psi}{\partial\alpha}\dot{\alpha} - \frac{1}{T}\mathbf{Q} \cdot \operatorname{Grad}(T) \geqslant 0 \tag{4.5}$$

The state equations for the Kirchhoff stress tensor and thermodynamic force conjugated to α are specified as

$$\boldsymbol{\tau} = 2\frac{\partial\psi}{\partial\mathbf{b}^r}\mathbf{b}^r \qquad h = \frac{\partial\psi}{\partial\alpha} \tag{4.6}$$

Now, the reduced form of dissipation inequality can be written

$$\mathcal{D} = \boldsymbol{\tau} : \mathbf{d}^p - h\dot{\alpha} - \frac{1}{T}\mathbf{Q} \cdot \operatorname{Grad}(T) \geqslant 0 \tag{4.7}$$

The total dissipation can be divided into mechanical and thermal contribution as follows

$$\mathcal{D}_{mech} = \boldsymbol{\tau} : \mathbf{d}^p - h\dot{\alpha} \geqslant 0 \qquad \mathcal{D}_{therm} = -\frac{1}{T}\mathbf{Q} \cdot \operatorname{Grad}(T) \geqslant 0 \tag{4.8}$$

Next, the energy balance equation in temperature form can be written for the thermo-elasto-
-plastic material

$$c\dot{T} + \text{Div}\,(\mathbf{Q}) = \underbrace{\mathcal{H} + \mathcal{D}_{mech} + \mathcal{A}}_{Q_{mech}} + \mathcal{R} \qquad c = -T\frac{\partial^2 \psi}{\partial T^2}$$

$$\mathcal{H} = \Big[T\frac{\partial \boldsymbol{\tau}}{\partial T}\Big] : [\mathbf{d} - \mathbf{d}^p] \qquad \mathcal{A} = T\frac{\partial h}{\partial T}\dot{\alpha} \tag{4.9}$$

In the above equation, Q_{mech} represents the mechanical heat production rate which consists of thermo-elastic heating/cooling $\mathcal{H}$, mechanical dissipation related to the plastic process $\mathcal{D}_{mech}$ and contribution $\mathcal{A}$ which is related to the temperature dependence of the thermodynamic force conjugated to the hardening variable.

In the subsequent analysis, we assume free energy $\psi = \psi^r(\mathbf{b}^r, T) + \psi^p(\alpha) + \psi^T(T)$ which is additively decoupled into reversible, plastic and purely thermal parts as follows, see (Ristinmaa *et al.*, 2007)

$$\psi^r = \frac{1}{2}K\ln^2(J) + \frac{1}{2}G\Big[\text{tr}\,([J^{br}]^{-1/3}\mathbf{b}^r) - 3\Big] - 3K\alpha_T(T - T_0)\ln(J)$$

$$\psi^p = \frac{1}{2}H\alpha^2 + [\sigma_{yf} - \sigma_{y0}]\Big[\alpha + \frac{1}{\delta}\exp(-\delta\alpha)\Big] \tag{4.10}$$

$$\psi^T(T) = c_0\Big[(T - T_0) - T\ln\Big(\frac{T}{T_0}\Big)\Big]$$

The introduction of the above specific form of the free energy allows for derivation of the thermodynamic force conjugated to the hardening variable as

$$h = H\alpha + [\sigma_{yf} - \sigma_{y0}][1 - \exp(-\delta\alpha)] \tag{4.11}$$

where σ_{y0} is the initial yield threshold, σ_{yf} is the final yield threshold and δ is a saturation constant. Moreover, the heat capacity from Eq. (4.9) remains constant $c = c_0$.

To complete the description of plasticity, the yield function and the flow rule have to be specified. In this work, the volume preserving Huber-Mises-Hencky yield function is applied

$$F_p(\boldsymbol{\tau}, \alpha, T) = f(\boldsymbol{\tau}) - \sqrt{\frac{2}{3}}\sigma_y(\alpha, T) \leqslant 0 \qquad f(\boldsymbol{\tau}) = \sqrt{\boldsymbol{\tau}_{dev} : \boldsymbol{\tau}_{dev}}$$

$$\boldsymbol{\tau}_{dev} = \boldsymbol{\tau} - \frac{1}{3}\text{tr}\,(\boldsymbol{\tau})\mathbf{I} \qquad \sigma_y(\alpha, T) = \Big[1 - H_T[T - T_0]\Big]\sigma_{y0} + h \tag{4.12}$$

where H_T is the thermal softening modulus and T_0 is the reference temperature.

The flow rule is defined through the Lie derivative of $\mathbf{b}^r$, cf. (Simo and Miehe, 1992)

$$-\frac{1}{2}\mathcal{L}_v\mathbf{b}^r = \dot{\gamma}\mathbf{N}^p\mathbf{b}^r \qquad \mathbf{N}^p = \frac{\partial F_p}{\partial \boldsymbol{\tau}}$$

where $\dot{\gamma}$ is a plastic multiplier related to the hardening variable by formula $\dot{\alpha} = \sqrt{2/3}\dot{\gamma}$.

Now, having the thermo-elasto-plastic model in hand, the structural sources of heating can be analysed in more detail. The thermo-elastic source of heat from Eq. (4.9) can be written as

$$\mathcal{H} = -3K\alpha_T[\text{tr}\,(\mathbf{d}) - \text{tr}\,(\mathbf{d}^p)] = -3K\alpha_T\Big[\frac{1}{J}\dot{J} - \frac{1}{J^p}\dot{J}^p\Big] \qquad J^p = \det(\mathbf{F}^p) \tag{4.13}$$

The yield function leads to $\dot{J}^p = 0$, so that the above equation can be rewritten as

$$\mathcal{H} = -3TK\alpha_T\text{tr}\,(\mathbf{d}) = -3TK\alpha_T\frac{1}{J}\dot{J} \tag{4.14}$$

The second structural source of heat, i.e. plastic dissipation, can be derived as

$$\mathcal{D}_{mech} = \underbrace{\boldsymbol{\tau} : \mathbf{d}^p}_{\dot{w}^p} - h\dot{\alpha} = \dot{\gamma}\Big[f - \sqrt{\frac{2}{3}}h\Big] = \sqrt{\frac{2}{3}}\dot{\gamma}\Big[1 - H_T[T - T_0]\Big]\sigma_{y0} \tag{4.15}$$

The fraction of rate of plastic work $\dot{w}^p$ which is converted into heat can be calculated as, cf. (Ristinmaa *et al.*, 2007)

$$\eta = 1 - \frac{h\dot{\alpha}}{\boldsymbol{\tau} : \mathbf{d}^p} = \frac{[1 - H_T[T - T_0]]\sigma_{y0}}{\sigma_y} \tag{4.16}$$

As it was mentioned in the introduction, an alternative estimation for the plastic dissipation often used in literature is, see e.g. (Wriggers *et al.*, 1992)

$$\mathcal{D}_{mech} = \chi\dot{w}^p = \chi[\boldsymbol{\tau} : \mathbf{d}^p] = \sqrt{\frac{2}{3}}\chi\dot{\gamma}\sigma_y \tag{4.17}$$

where χ is the fraction of rate of plastic work converted into heat, often called the Taylor--Quinney coefficient, which is usually assumed to be a constant material parameter with value from interval 0.8-0.95.

4.2. Numerical simulations for thermo-elasto-plasticity

Numerical verification of the presented thermo-elasto-plastic model is performed similarly to the thermo-elasticity using two specimens: the cube presented in Fig. 1a and the dogbone sample, see Fig. 2. The main attention is now paid to the influence of transition from the elastic to plastic regime on the temperature change in the sample and the impact of the applied formulation of plastic dissipation, in particular plastic dissipation calculated:
   a) straightforwardly from thermodynamic, i.e. using Eq. (4.15), called further *Model 1*
   b) using Taylor-Quinney coefficient according to Eq. (4.17) called further *Model 2*.

Both samples are simulated using the same material properties. The elastic and thermal parameters related to aluminium are taken from Section 3.2.1, whereas the parameters describing the plastic behaviour are as follows: $\sigma_{y0} = 150 \cdot 10^6$ Pa, $\sigma_{yf} = 390 \cdot 10^6$ Pa, $H = 0$, $\delta = 12$, $H_T = 0.0016\,\mathrm{K}^{-1}$. For Model 2, the value of the Taylor-Quinney coefficient equals $\chi = 0.9$.

4.2.1. Uniaxial tension test

The cubic sample from Fig. 1a is now elongated by $\Delta L = 1\,\mathrm{mm}$ within $16.7\,\mathrm{s}$ which gives the displacement rate equal to $6 \cdot 10^{-5}$ m/s. The results obtained in simulations are presented in Fig. 5. The diagram presenting the sum of reactions (Fig. 5a) shows that the onset of plasticity takes place when $t/t_{proc} = 0.02$ and from this point the diagram related to plasticity with significant strain hardening is observed. The reactions are very close for the two applied models of plastic dissipation, however, differences are observed for the temperature diagram in Fig. 5b. In this case, Model 1 manifests higher temperature in the sample at the beginning of the plastic process and lower in the second part, and this is consistent with the amount of dissipated energy during the process, cf. Fig. 5c. As the elongation progresses, the difference in the plastic dissipation for the two models becomes greater. In the last diagram presented in Fig. 5, the fraction of the plastic work converted into heat is presented for the two analysed models. For Model 1, the fraction with coefficient η defined in Eq. (4.16) is shown. It can be observed that the constant fraction of the plastic work defined by coefficient χ used in Model 2 can be treated as an average of the fraction calculated with Model 1 for the initial part of plastic deformation (for the whole process the averaged value of η is lower than the applied value of χ).

It is worth noting that in the elastic regime the thermo-elastic cooling is properly reproduced as a decrease in temperature at the beginning of the process, see Fig. 5b. The onset of plasticity can also be recognized as the moment at which temperature in the sample starts to grow.
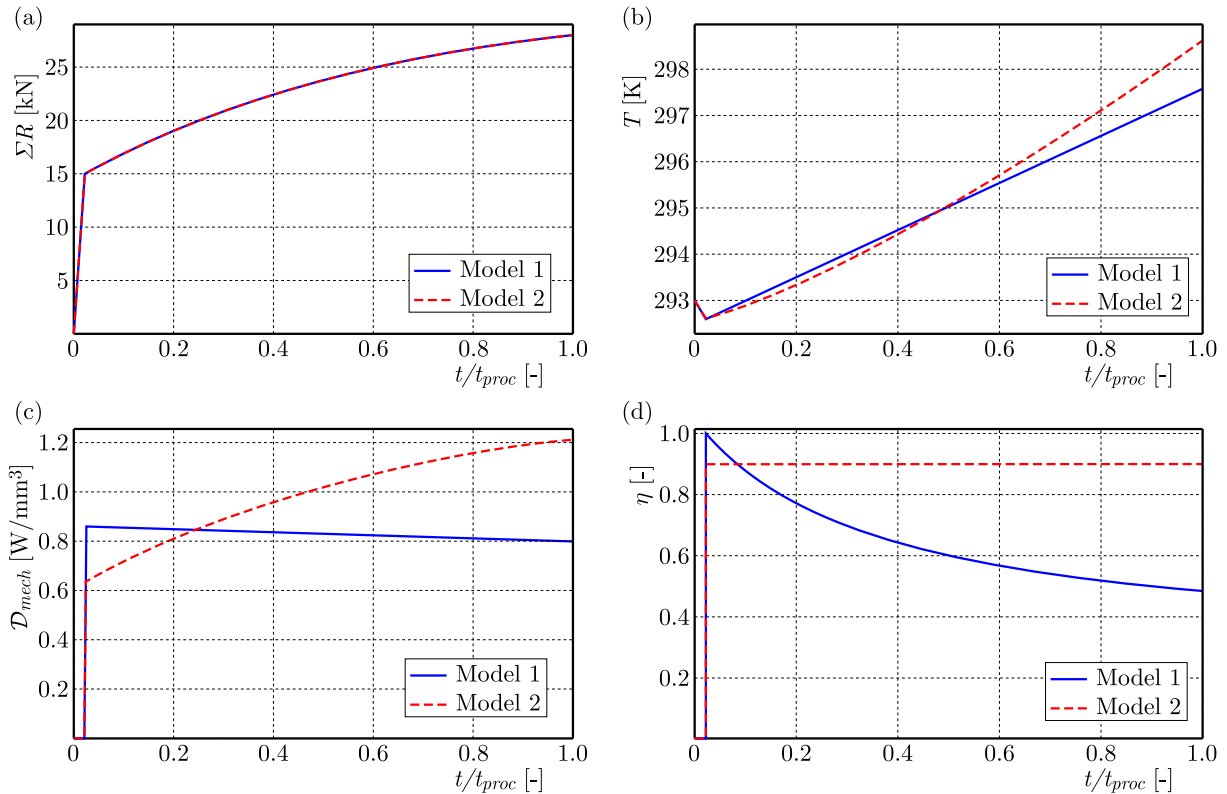
Fig. 5. Results for the uniaxial tension test for thermo-elasto-plasticity: (a) sum of reactions, (b) temperature, (c) plastic dissipation, (d) fraction of plastic work converted into heat source

4.2.2. Dogbone sample – comparison with experiment for elasto-plasticity

The dogbone sample is elongated now with the displacement rate $6 \cdot 10^{-5}$ m/s. The simulations are performed for the slow process due to the fact that the plasticity description does not include viscosity, which can have a significant impact on the results for faster deformation. The results of computational tests for the dogbone specimen are presented in Fig. 6. At the initial stage of the plastic process, see Fig. 6a, a slight softening and plateau in the diagram is visible. This behaviour is related to the formation and expansion of Lueders bands. The material model which is used in the simulation does not reproduce this phenomenon, however, it correctly it simulates the onset of plasticity and the overall plastic behaviour until the failure, see Fig. 6b. The oscillations visible in the experimental diagrams in Fig. 6b are a result of the PLC effect. The differences between Model 1 and Model 2 are negligible in the displacement-force diagram, however the choice of the model has a significant influence on temperature evolution, see Fig. 7. Model 1, which predicts plastic dissipation directly from thermodynamics, shows higher temperature at the beginning of the plastic process and lower in the following part of the process with respect to Model 2. The analysis of the diagrams in Fig. 7 clearly shows that Model 1 is closer to the experimental results.

Note that the temperature evolution in the elastic regime is very close to experimental measurements and, what is of great importance, the increase of temperature starts in simulations and experiments exactly at the same moment. Thus the analysis of temperature evolution (the end of elastic cooling) allows for detection of plasticity onset.

The deformed samples with temperature distribution in the middle of the elongation process (enforced displacement equals 15 mm) are depicted in Fig. 8. Both the plots of temperature, obtained with Model 1 and Model 2, are presented using the same scale, which allows for a
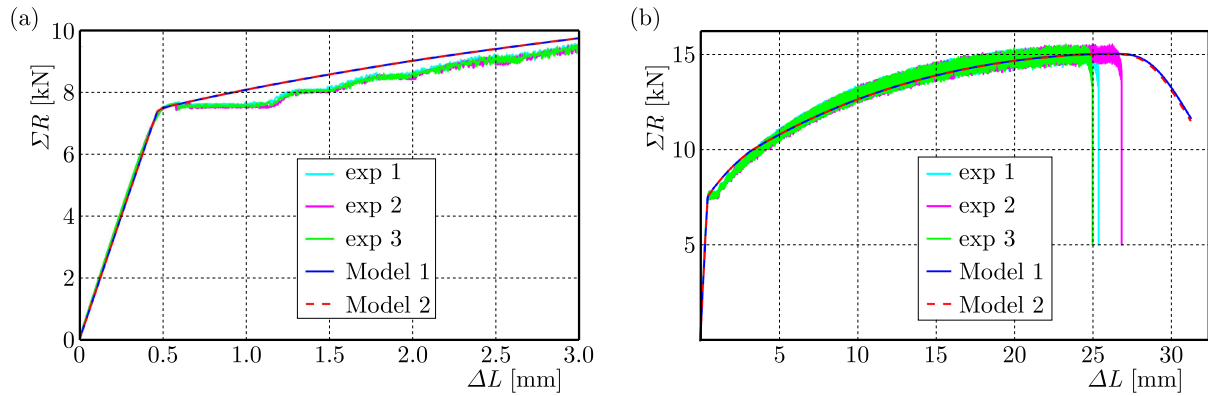
Fig. 6. Sum of reactions vs. enforced displacement: (a) initial stage, (b) whole process
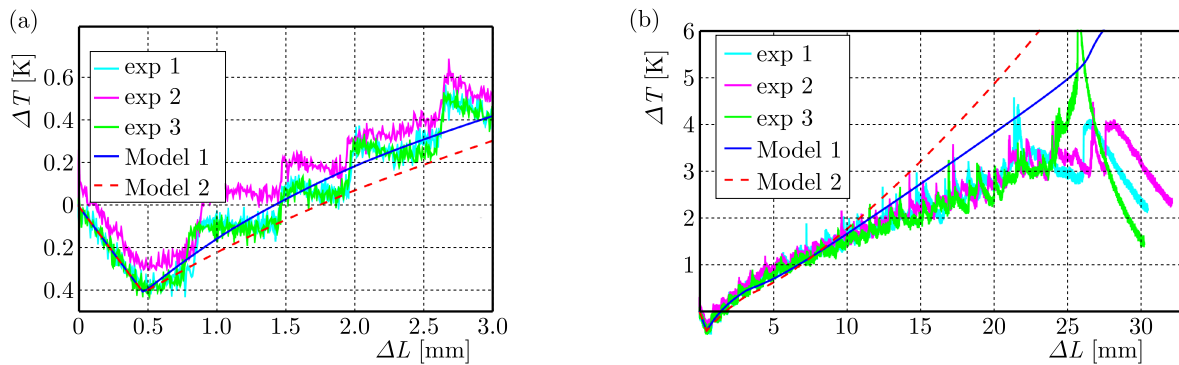

Fig. 7. Temperature at the central point of the sample vs. enforced displacement: (a) initial stage, (b) whole process
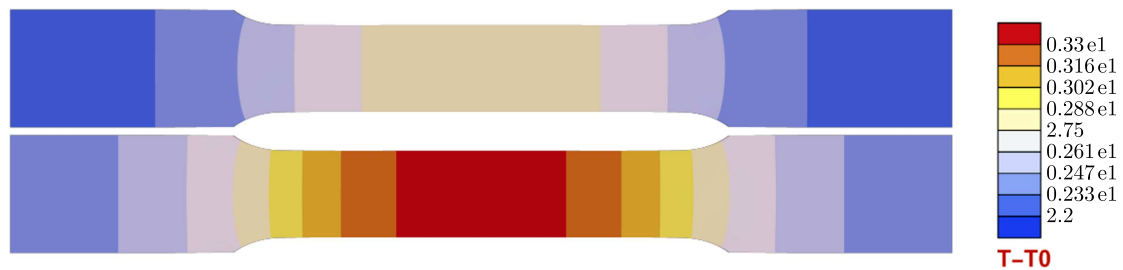

Fig. 8. Deformed mesh with temperature distribution in the middle of the deformation process for Model 1 (top) and Model 2 (bottom)

comparison. Model 2 manifests significantly higher temperatures in the sample than Model 1. For both models, the highest temperature is located in the central part of the sample and it is a precursor of necking.

5.   Conclusion

The paper is focused on internal heat sources observed in large strain thermo-elastic and thermo--elasto-plastic materials. It includes description of material models and presentation of numerical simulations with remarks aimed at deeper understanding of the phenomena. Computations have been performed using AceGen/AceFEM packages in Wolfram Mathematica, starting from a one-element test. Then a dogbone-shape sample has been analysed, for which the results have been compared with experimental ones.

In the elastic regime, the presented and implemented model reproduces thermo-elastic cooling characteristics for metals, e.g. for aluminium, which is in general a rate-dependent phenomenon. However, it has been shown in the analysis of uniaxial tension tests that for samples with homogeneous temperature distribution the diagrams do not depend on the tension rate. Experimental and computational results for the dogbone sample show a good agreement for both the sum of reactions and temperature diagrams, even though there is no direct material parameter to control the cooling rate in the model.

For the plastic material, the attention has been focused on the heating source related to plastic dissipation. Two models have been used, Model 1 in which dissipation is calculated directly from thermodynamic derivation and Model 2 where estimation of plastic dissipation is obtained using the Taylor-Quinney coefficient. The force-displacement diagrams for the two thermo-elasto-plastic models overlap, however, the diagrams of temperature differ from the beginning of the plastic process, which is a result of different amount of dissipated energy in the two analysed models. Overall, good agreement between experimental and computational results has been obtained, and Model 1 gives results closer to experimental ones especially for the advanced stage of the process.

The incorporation of thermo-elastic coupling in the thermo-elasto-plastic model allows one to recognize the beginning of the plastic process at a material point, and the presented simulations properly reproduce the transition from elastic to plastic regime observed in the experimental sample.

References

1. BONET J., WOOD R.D., 3008, *Nonlinear Continuum Mechanics for Finite Element Analysis*, 2nd ed., Cambridge University Press, Cambridge

2. DE SOUZA NETO E.A., PERIC D., OWEN D.R.J., 2008, *Computational Methods for Plasticity. Theory and Applications*, John Wiley & Sons, Chichester, UK

3. DUSZEK M., PERZYNA P., 1991, The localization of plastic deformation in thermoplastic solids, *International Journal of Solids and Structures*, **27**, 11, 1419-1443

4. HAUPT P., 2002, *Continuum Mechanics and Theory of Materials*, Springer

5. HOLZAPFEL G.A., 2000, *Nonlinear Solid Mechanics. A Continuum Approach for Engineering*, John Wiley & Sons, Chichester

6. KORELC J., WRIGGERS P., 2016, *Automation of Finite Element Methods*, Springer International Publishing Switzerland

7. MARSDEN J.E., HUGHES T.J.R., 1983, *Mathematical Foundations of Elasticity*, Dover Publications, Inc., New York

8. MUCHA M., ROSE L., WCISŁO B., MENZEL A., PAMIN J., 2023, Experiments and numerical simulations of Lueders bands and Portevin-Le Chatelier effect in aluminium alloy AW5083, *Archives of Mechanics*, **75**, 3, 301-336

9. MUSIAŁ S., MAJ M., URBAŃSKI L., NOWAK M., 2022, Field analysis of energy conversion during plastic deformation of 310S stainless steel, *International Journal of Solids and Structures*, **238**, 1, 111411

10. OLIFERUK W., MAJ M., ZEMBRZYCKI K., 2013, Determination of the energy storage rate distribution in the area of strain localization using infrared and visible imaging, *Experimental Mechanics*, **55**, 4, 753-760

11. OPPERMANN P., DENZER R., MENZEL A., 2022, A thermo-viscoplasticity model for metals over wide temperature ranges – application to case hardening steel, *Computational Mechanics*, **69**, 541-563

12. RISTINMAA M., WALLIN M., OTTOSEN N.S., 2007, Thermodynamic format and heat generation of isotropic hardening plasticity, *Acta Mechanica*, **194**, 103-121

13. ROSE L., MENZEL A., 2021, Identification of thermal material parameters for thermo-mechanically coupled material models, *Meccanica*, **56**, 393-416

14. SIMO J.C., 1998, Numerical analysis and simulation of plasticity, [In:] P.G. Ciarlet and J.L. Lions, Edit., *Handbook of Numerical Analysis. Numerical Methods for Solids (Part 3)*, Vol, VI, 183-499, Elsevier Science, Boca Raton

15. SIMO J.C., HUGHES T.J.R., 1998, *Computational Inelasticity. Interdisciplinary Applied Mathematics*, Vol. 7, Springer-Verlag, New York

16. SIMO J.C., MIEHE C., 1992, Associative coupled thermoplasticity at finite strains: Formulation, numerical analysis and implementation, *Computer Methods in Applied Mechanics and Engineering*, **98**, 1, 41-104

17. TAYLOR G.I., QUINNEY H., 1934, The latent energy remaining in a metal after cold working, *Proceedings of the Royal Society of London. Series A*, **143**, 307-326

18. TRUESDELL C., TOUPIN R.A., 1960, The classical field theories, [In:] S. Flügge, Edit., *Encyclopedia of Physics. Vol. III Principles of Classical Mechanics and Field Theory*, 226-788, Springer-Verlag, Berlin Heidelberg

19. WCISŁO B., PAMIN J., 2017, Local and non-local thermomechanical modeling of elastic-plastic materials undergoing large strains, *International Journal for Numerical Methods in Engineering*, **109**, 1, 102-124

20. WCISŁO B., PAMIN J., ROSE L., MENZEL A., 2023, On spatial vs. referential isotropic Fourier's law in finite deformation thermomechanics, *Engineering Transactions*, **71**, 1, 111140

21. WRIGGERS P., 2008, *Nonlinear Finite Element Methods*, Springer-Verlag, Berlin Heidelberg

22. WRIGGERS P.A., MIEHE C., KLEIBER M., SIMO J.C., 1992, On the coupled thermomechnical treatment of necking problems via finite element methods, *International Journal for Numerical Methods in Engineering*, **33**, 869-883

23. ZIENKIEWICZ O.C., TAYLOR R.L., ZHU J.Z., 2005, *The Finite Element Method: Its Basis and Fundamentals*, 6th ed., Elsevier Butterworth-Heinemann